Understanding protein complex formation: the role of charge distribution in the encounter complex

Di Savino, A.

Chapter 5

Enhancing the population of encounter complex affects protein complex formation efficiency.

Based on the research article:

Di Savino, A. and Ubbink, M. Enhancing the population of encounter complex affects protein complex formation efficiency, *Under revision.*

Abstract

Optimal charge distribution is considered to be important for efficient formation of protein complexes. Electrostatic interactions guide encounter complex formation that precedes the formation of an active protein complex. However, disturbing the optimized distribution by introduction of extra charged patches on cytochrome *c* peroxidase does not lead to a reduction in productive encounters with its partner cytochrome *c*. To test whether a complex with a high population of encounter complex is more easily affected by suboptimal charge distribution, the interactions of cytochrome *c* mutant R13A with wild type cytochrome *c* peroxidase and a variant with an additional negative patch were studied. The complex of the peroxidase and cytochrome *c* R13A was reported to have an encounter state population of 80%, compared to 30% for the wild type cytochrome *c*. NMR analysis confirms the dynamic nature of the interaction and demonstrates that the mutant cytochrome *c* samples the introduced negative patch. Kinetic experiments show that productive complex formation is 5-7 fold slower at moderate and high ionic strength values for cytochrome *c* R13A but the association rate is not affected by the additional negative patch on cytochrome *c* peroxidase, showing that the total charge on the protein surface can compensate for less optimal charge distribution. At low ionic strength (44 mM), the association with the mutant cytochrome *c* reaches the same high rates as found for wild type cytochrome *c*, approaching the diffusion limit.

Introduction

Electrostatic interactions play a major role in protein complex formation. The collision of free proteins in solution can result in early dissociation or lead to the formation of the stereospecific and active complex. Electrostatic interactions can promote the interactions between proteins, guiding the formation of an encounter complex.[1–5] The encounter complex is a very dynamic ensemble of configurations in which proteins sample each other's surface.[6] It can lead to the formation of the stereospecific and active complex, in which case the encounter is productive.[7] In case of an early dissociation, the encounter is futile.[8] The charge distribution on the surface is considered to be critical to enhance the number of productive encounters, by guiding the incoming partner to the binding site and reducing the surface area to be searched.[9] Previous studies showed how charge mutations can affect the interactions between proteins. For example, on the complex formed by TEM1-β-lactamase (TEM1) and its inhibitor, β-lactamase-inhibitor protein (BLIP), charge mutations can enhance the formation of the productive encounter complex resulting in a higher association rate (k_a) but without lowering the dissociation rate. Alternatively, they can alter the encounter complex without any effect on the k_a, or improve the k_a without affecting the encounter complex.[7] Charge mutations can modify the balance of productive and futile encounter complexes, even if located far from the stereospecific binding site. The outcome of the mutation depends on

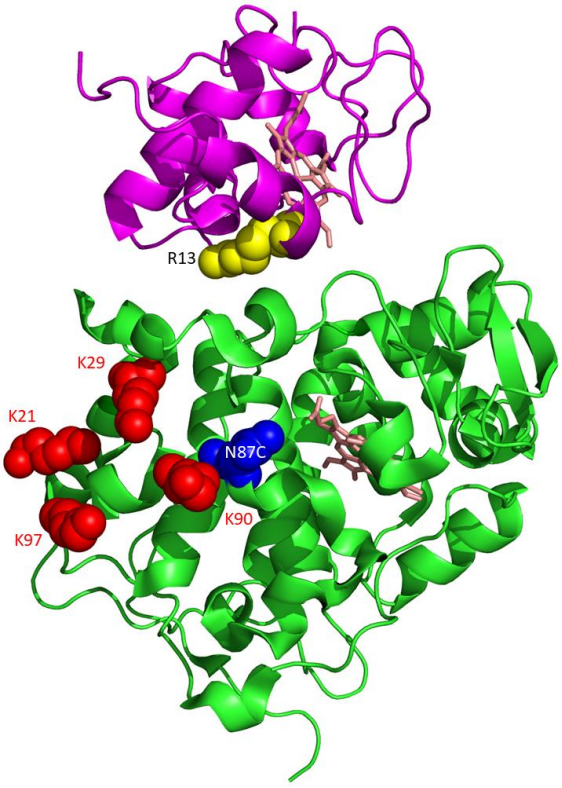

Figure 5.1. Mutations in the Cc:CcP complex. The crystal structure of the stereospecific complex formed by Cc (magenta ribbons) and CcP (green ribbons) is shown (PDB 2PCC[13]). The heme groups are shown in salmon sticks, residue R13 is indicated in yellow spacefill representation, the Lys residues that were mutated to Glu to introduce additional negative charges in CcP_B are indicated in red, and residue N87 of CcP mutated to cysteine for spin labelling in blue spacefill. The figure was made with Pymol[12].

the optimization or interruption of favorable electrostatic 'pathways'.[10] The effect of the charged pathways was observed for the complex of cytochrome P450cam and putidaredoxin.[11]

Because of their biological functions, electron transfer (ET) proteins often form transient complexes and the charge distribution on their surface is highly optimized to have favorable electrostatic interactions, leading to efficient protein complex formation. These complexes usually have low affinity (K_D in the μM-mM range), a consequence of the association and dissociation rate constants both being high. Protein complexes with highly optimized electrostatic interactions have k_a values that approach the limit set by translational diffusion.[1] The ET complex formed by cytochrome *c* (Cc) and cytochrome *c* peroxidase (CcP) from baker's yeast (*Saccharomyces cerevisiae*) is one of the most studied and best characterized ET complexes. The formation of the complex is guided by electrostatic interactions between the positively charged binding site on Cc and the negatively charges on CcP.[13–17] The encounter state represents 30% of the complex, while 70% is in the stereospecific complex and Cc samples merely 15% of the surface of CcP.[18,19] Several studies have shown that mutations in the interface between Cc and CcP strongly affect association,[20–22] so we wondered how important the optimized charge distribution is for the efficiency of the ET reaction. To test this, negative patches were added distant from the stereospecific binding site on CcP, enlarging the surface sampled by Cc in the encounter state. Interestingly, the new negative charges create productive encounters, slightly enhancing the k_a, even if located far from the stereospecific binding site ([23] and [24]). This suggests that the overall charge on CcP surface is more important than the charge distribution. We considered that this could be a consequence of the stability of the stereospecific state as compared to the encounter state. To test this idea, for the current work, we turned to a mutant of Cc, R13A, reported to form a complex with Cc with 80% population of the encounter state.[25] Arg13 has been shown to be a hot-spot in the interactions of the stereospecific complex and its mutation to Ala shifts the balance toward the encounter state and reduces the affinity by 30 fold.[25,26] This mutant was used to study the interaction with native CcP (CcP_A) and a variant with eight additional negative charges on the side of CcP relative to the stereospecific binding site (CcP_B, Figure 5.1)([23] and [24]). Chemical shift perturbation (CSP) analysis and paramagnetic relaxation enhancement (PRE) experiments show that the complex is highly dynamic and that Cc visits the new negative patch in CcP_B. Kinetic experiments yield reduced association rates for the mutant Cc at moderate and high ionic strength values, but surprisingly, the addition of the negative patch does not reduce the number of productive encounters. At low ionic strength, the mutant Cc associates as fast as wild type (wt) Cc with CcP. The results are discussed in the context of the importance of charge optimization for complex formation.

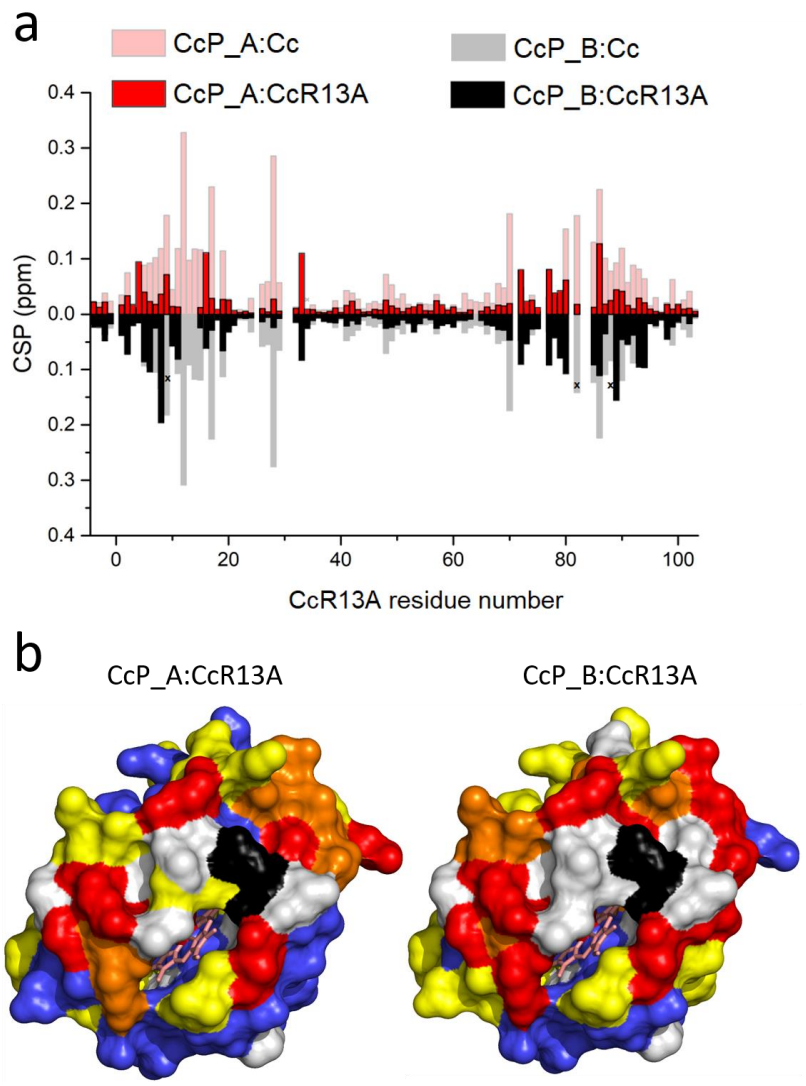

Figure 5.2. CSP upon complex formation. a) Comparison between the average CSP for the complexes CcP_A:Cc R13A (in red), CcP_B:Cc R13A (in black), CcP_A:wt Cc (in red shading) and CcP_B:wt Cc (in grey).[23] The black crosses indicate residues for which data are not available; b) CSP map for ^{15}N Cc R13A in complex with CcP_A (left) and CcP_B (right). The surface model of Cc (PDB 2PCC[13], haem in salmon sticks) is colored according to the code: residues with $\Delta\delta_{avg} \geq 0.06$ ppm are red, 0.04-0.06 ppm are orange, 0.02-0.04 ppm are yellow, <0.02 ppm are blue, the residues for which no data are available are light gray and residue R13 is black (See Table S5.1 for the list of red, orange and yellow residues).

Results

The Cc R13A – CcP interaction is predominantly in the encounter state. Binding to CcP causes considerable changes in the amide chemical shifts of Cc.[27] These changes are thought to be caused predominantly by the stereospecific complex. In this state, Cc is partly desolvated and engages in specific interactions, whereas in the encounter complex Cc is thought to remain solvated and assume multiple orientations.[28] Cc R13A was shown to shift the equilibrium between encounter and stereospecific states toward the former.[25] In line with those findings, the chemical shift perturbations (CSP) observed for the ^{15}N Cc R13A binding to CcP_A are much smaller than those for wt Cc (Figure 5.2a, red bars). Also upon binding to CcP_B the CSP remain overall smaller for Cc R13A than for wt Cc, indicating that the complex is mainly in the encounter state. Cc R13A interacts with the same surface to CcP_A and CcP_B (Figure 5.2b) but some differences can be observed. The CSP pattern shows several larger perturbations when binding to CcP_B (in the region of residues 5-10 and around residue 90), suggesting the formation of several more specific interactions.

Cc R13A binds the new patch on CcP_B. To establish whether the introduction of the added negative charges in CcP_B influence the encounter complex with Cc R13A, PRE experiments were performed. CcP_A and CcP_B were tagged with the spin label MTSL after mutating residue N87, which is located close to the added negative patch (Figure 5.1), to cysteine. The tag causes enhanced relaxation for nuclear spins in ^{15}N labelled Cc R13A

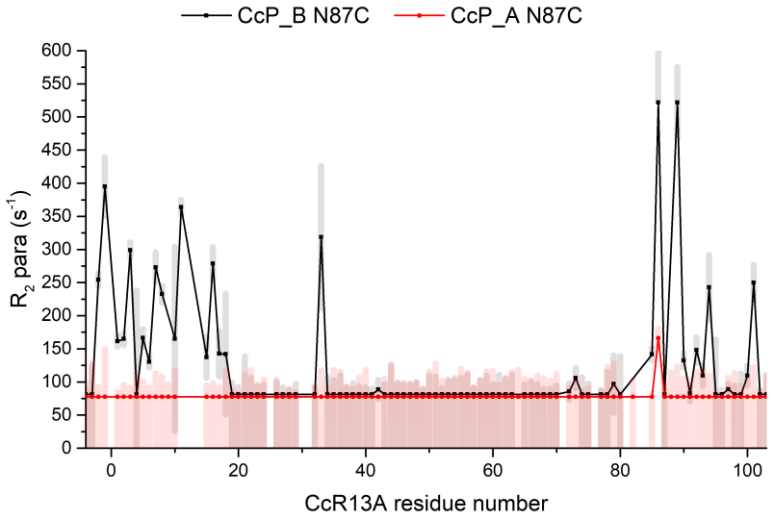

Figure 5.3. Probing new interactions with PRE NMR. The PREs are shown for amide nuclear spins of Cc R13A in presence of CcP_A (in red) or CcP_B (in black), tagged with MTSL at Cys87, which is located close to the negative patch added on CcP_B. The error bars are indicated as shaded regions and represent the propagated 2× SD errors of the raw data. The observed PREs were divided by 0.15 to correct for the fraction of CcP that was paramagnetic (see text).

that come within ~2.5 nm of the tag during the interactions with CcP. EPR experiments show that only 15% of the MTSL remained paramagnetic during the tagging reaction (and remains stable afterward). We have observed before that MTSL gets partly reduced during the reaction with CcP so routinely the paramagnetic fraction is established by EPR. The interaction of Cc with CcP is very fast on the NMR timescale so all Cc molecules sample many CcP molecules rapidly, averaging the effect of interactions with diamagnetic and paramagnetic CcP molecules. Figure 5.3 presents the observed PRE for the amides of Cc R13A upon interacting with CcP_A and CcP_B labelled at Cys87 with MTSL. The PREs have been corrected for the 15% paramagnetic labelling by dividing the observed PREs by 0.15. In CcP_A significant PRE signal was observed for only one aminoacidic residue, indicating that Cc R13A does not interact with the surface close to N87. Upon complex formation with CcP_B, large PREs are observed, indicating that Cc R13A visits the region with the extra charges in proximity of the paramagnetic tag on CcP_B. Clearly, the encounter complex includes the new patch on CcP_B, in line with the findings for wt Cc.[23]

Cc R13A reacts more slowly with CcP. To determine whether the R13A mutation in Cc influences the association rate constant with CcP, it was measured as a function of the ionic strength using stopped-flow measurements. Following the work of Miller et al. (1994),[29] the association rate constant can be measured by observing ET from Cc(Fe^{2+}) to CcP compound I (CpdI). The ET rate constant is high, so the observed second order rate constant is a lower-limit estimate of the association rate constant, as explained in detail in a

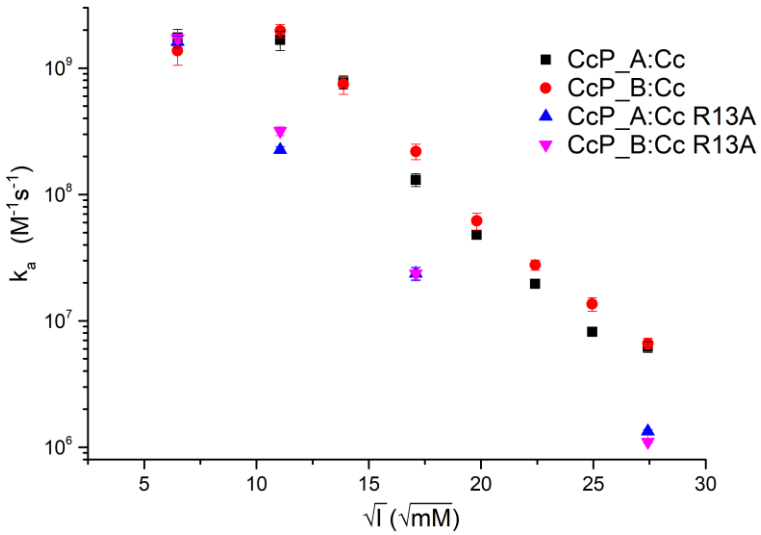

Figure 5.4. Rate of association (k_a) between the Cc and CcP variants. The k_a values, plotted as a function of the square root of the ionic strength, were obtained from the simulations of the stopped flow kinetics. Errors were calculated as the standard deviation between replicates and simulations performed at different CcP concentrations (see Materials and Methods of [24] for details).

previous paper.[24] The association rate constant for wt Cc to CcP_A and CcP_B is strongly dependent on the ionic strength (Figure 5.4, data reproduced from ref [23] and [24]), due to the favorable electrostatic interactions between the Cc and CcP surfaces.[30–34] Following the same approach, the association rate constant (k_a) was measured for Cc R13A and CcP_A or CcP_B. In a wide range of ionic strength values, from 122 mM (11 $mM^{1/2}$ on the axis of Figure 5.4) to 730 mM (27 $mM^{1/2}$), the k_a of the complexes formed by Cc R13A are 5-7 fold lower than for the complexes formed by wt Cc (Tables S5.2, S5.3 and S5.4). However, curiously, at the lowest ionic strength tested, 44 mM (7 $mM^{1/2}$) the k_a of the Cc R13A complexes reaches the same level as those for the complexes formed by wt Cc. Before, the surprising observation was made that the introduction of a strong negative patch on CcP distant from the stereospecific binding site did not lower the k_a for wt Cc, but rather increased it somewhat.[24] Similarly, for Cc R13A, we observe that the formation of the ET active complex is not slowed down by the additional charges on CcP_B, as compared to CcP_A.

Discussion

Volkov *et al.*[25] showed that the Cc mutation Arg13 to Ala drastically increases the population of the encounter complex with CcP, from 30% to 80%. Also, the binding constant (K_B) decreases from 1.9 * 10^5 M^{-1} of the wt complex to 0.06 * 10^5 M^{-1} for Cc R13A bound to CcP. We previously reported that the addition of a negative patch on a side of the binding site of CcP (CcP_B) enlarges the area sampled by Cc in the encounter complex. Since the k_a for Cc and CcP_B is slightly higher than that for the wt complex, it was concluded that the added charges result in more productive encounters.[23] The aim of the present study was to investigate to what degree the delicate balance between stereospecific complex and encounter complex influences the association between Cc and CcP by comparing the interactions between CcP with wt Cc and Cc R13A.

The CSP analysis shows that Cc R13A forms a much more dynamic complex with both CcP_A and CcP_B, than does wt Cc, in line with a more populated encounter state. The Cc R13A CSP patterns obtained with the two variants of CcP are not the same, contrary to the finding for wt Cc.[23] In the latter, the stereospecific complex is more populated and the main contributor to the CSP. The CSP differences observed for Cc R13A indicate differences in the interactions with CcP_A and CcP_B. This observation is further supported by the PRE results that show clearly that the region with the new negative patch in CcP_B is visited by Cc R13A. It does not do so in CcP_A, in accord with the Monte Carlo simulations reported in ref. [25], which showed that the encounter complexes of wt Cc and Cc R13A with CcP_A are very similar and comprise the surface area of CcP around the stereospecific binding site.

To test to what degree the increased dynamics in the complexes formed by Cc R13A influence the formation of the active complex, the k_a for binding to CcP_A or CcP_B was determined. The favorable electrostatic interactions between Cc R13A and the CcP variants cause a strong ionic strength dependence of k_a. At an ionic strength of 122 mM and higher,

the k_a values for the complexes formed by Cc R13A are 5-7 fold lower than for wt Cc at the same ionic strength. Surprisingly, at the lowest ionic strength tested, 44 mM, the k_a of the complexes formed by Cc R13A and either CcP variants reaches the k_a of the complexes formed by wt Cc. So, whereas the rate constant plateaus at low ionic strength for wt Cc, the one for Cc R13A monotonically increases.

The plateau reached for wt Cc can have various reasons. It could be that monopole-dipole interactions may come into play[35,36] at low ionic strength that work against each other and causing the leveling off of the k_a. However, this effect is observed for CcP_A and CcP_B and even for CcP_D, which has a strong new negative patch at the far end from the stereospecific binding site.[24] These three variants have widely different dipoles, yet all show the same behavior. Alternatively, the diffusion limit may be reached, so increasing charge interactions further does not result in faster association. A third explanation is that the encounter complex, which is dominated by electrostatic interactions is most favorable at low ionic strength and thus, the balance between encounter and stereospecific complex shifts to the former at low ionic strength, reducing the rate of formation of the active complex. Such 'inhibition' by strong charge interactions outside the stereospecific binding site has been proposed before.[37–40] It is not trivial to determine which of the latter two explanations is applicable here. We used simulation of complex formation to evaluate ranges that the k_a values can assume.

$$\mathrm{Cc(Fe^{2+})} + \mathrm{CpdI} \underset{k_{-1}}{\overset{k_1}{\rightleftarrows}} \text{Encounter complex} \underset{k_{-2}}{\overset{k_2}{\rightleftarrows}} \text{Stereospecific complex} \xrightarrow{k_{et}} \mathrm{Cc(Fe^{3+})}\text{:CpdII} \qquad \text{reaction 1}$$

The association reaction can be described by reactions 1, in which CpdII refers to compound II, the second intermediate in the reduction of hydrogen peroxide by CcP. Cc and CcP associate to form the encounter complex, which can evolve to the stereospecific complex in which ET can occur. At I = 122 mM, the K_B value, the population of the encounter complex and the k_a values have been reported for both wt Cc and Cc R13A in complex with CcP_A,([24,25], this work) restraining the microscopic rate constants in reaction 1. Details are given in the supporting information (Text S5.1) and Table S5.5 gives estimated values. Simulation shows that the 7-fold lower k_a value observed for Cc R13A is attributable to a combination of a lower k_1 and the lower population of the stereospecific complex (implying that the second equilibrium is more to the left). Cc R13A lacks the positive side chain of Arg13 in the binding interface, so a lowered k_1 is to be expected, because of weaker electrostatic interactions. The k_a observed for Cc R13A at 44 mM can be found by increasing k_1 and lowering k_{-1} without changing the population of the encounter state. For wt Cc, it could be that the k_1 obtained at I = 122 mM (2×10^9 $M^{-1}s^{-1}$ for CcP_A) represents the diffusion limit and cannot increase further at I = 44 mM. If it does increase, it must be accompanied by a substantially increased population (from 30% to >90%) of the encounter state to obtain the experimental k_a value, which is nearly the same as the one at I = 122 mM (Table S5.5). In summary, these simulation data do not allow to favor one of these explanations. This analysis shows that the lower association rate constant of Cc R13A

is due to reduced electrostatic interactions and less favorable binding at the stereospecific complex. At low ionic strength this difference with wt Cc is eliminated, because of the plateau reached by k_a of wt Cc.

Conclusions

Our CSP data confirm that the mutation of the Arg 13 of Cc to Ala enhances the dynamic component in the binding with the CcP variants. While it was shown that the binding mode of wt Cc with CcP_A and CcP_B is the same,[23] the interactions of Cc R13A with CcP_B differ more from those with CcP_A and are somewhat more specific. Paramagnetic relaxation enhancement (PRE) experiments showed that, similarly to what shown for the Cc:CcP_B complex,[23] the added charges enlarge the surface of CcP visited by Cc R13A. The new patch disturbs the optimized charge distribution on the surface of CcP, yet it does not result in less productive encounters because the association rate constant is not reduced. Stopped flow experiments were used to evaluate the influence of the higher population of encounter state on the association rate between Cc R13A and the CcP variants. At ionic strength values above 122 mM (11 $mM^{1/2}$), the k_a exhibits a 5-7 fold reduction compared to wt Cc, indicating that the population of the encounter state has a role in balancing dynamics and specificity in the protein complex formation, and thus can be critical for the efficiency of ET.

References

(1) Schreiber, G., Haran, G., and Zhou, H. X. (2009) Fundamental aspects of protein-protein association kinetics. *Chem. Rev. 109*, 839–860.

(2) Ubbink, M. (2012) Dynamics in transient complexes of redox proteins. *Biochem. Soc. Trans. 40*, 415–418.

(3) Yang, J., Zeng, Y., Liu, Y., Gao, M., Liu, S., Su, Z., and Huang, Y. (2020) Electrostatic interactions in molecular recognition of intrinsically disordered proteins. *J. Biomol. Struct. Dyn.* Taylor and Francis Ltd.

(4) Zhou, H. X., and Pang, X. (2018) Electrostatic interactions in protein structure, folding, binding, and condensation. *Chem. Rev.* American Chemical Society.

(5) Clore, G. M. (2014) Interplay between conformational selection and induced fit in multidomain protein-ligand binding probed by paramagnetic relaxation enhancement. *Biophys. Chem.* Elsevier B.V.

(6) Schilder, J., and Ubbink, M. (2013) Formation of transient protein complexes. *Curr. Opin. Struct. Biol. 23*, 911–918.

(7) Harel, M., Spaar, A., and Schreiber, G. (2009) Fruitful and futile encounters along the association reaction between proteins. *Biophys. J. 96*, 4237–4248.

(8) Fawzi, N. L., Doucleff, M., Suh, J. Y., and Clore, G. M. (2010) Mechanistic details of a

protein-protein association pathway revealed by paramagnetic relaxation enhancement titration measurements. *Proc. Natl. Acad. Sci. U. S. A. 107*, 1379–1384.

(9) Adam, G., and Delbrück, M. (1968) Reduction of dimensionality in biological diffusion processes, in *Structural Chemistry and Molecular Biology* (A. Rich, N. D., Ed.), p 198. W. H. Freeman and Co., San Francisco.

(10) An, S. Y., Kim, E.-H., and Suh, J.-Y. (2018) Facilitated protein association via engineered target search pathways visualized by paramagnetic NMR spectroscopy. *Structure 26*, 887-893.e2.

(11) Andrałojć, W., Hiruma, Y., Liu, W. M., Ravera, E., Nojiri, M., Parigi, G., Luchinat, C., and Ubbink, M. (2017) Identification of productive and futile encounters in an electron transfer protein complex. *Proc. Natl. Acad. Sci. U. S. A. 114*, E1840–E1847.

(12) Schrödinger, L. The PyMOL molecular graphics system, Version 1.3.

(13) Pelletier, H., and Kraut, J. (1992) Crystal structure of a complex between electron transfer partners, cytochrome *c* peroxidase and cytochrome *c*. *Science (80-.). 258*, 1748–1755.

(14) Gabdoulline, R. R., and Wade, R. C. (2001) Protein-protein association: investigation of factors influencing association rates by Brownian dynamics simulations. *J. Mol. Biol. 306*, 1139–1155.

(15) Poulos, T. L., Freer, S. T., Alden, R. A., Edwards, S. L., Skogland, U., Takio, K., Eriksson, B., Xuong, N. H., Yonetani, T., and Kraut, J. (1980) Crystal-structure of cytochrome-c peroxidase. *J. Biol. Chem. 255*, 575–580.

(16) Louie, G. V, Hutcheon, W. L. B., and Brayer, G. D. (1988) Yeast iso-1-cytochrome c: A 2.8 Å resolution three-dimensional structure determination. *J. Mol. Biol. 199*, 295–314.

(17) Northrup, S. H., Boles, J. O., and Reynolds, J. C. (1988) Brownian dynamics of cytochrome *c* and cytochrome *c* peroxidase association. *Science (80-.). 241*, 67–70.

(18) Volkov, A. N., Worrall, J. A. R., Holtzmann, E., and Ubbink, M. (2006) Solution structure and dynamics of the complex between cytochrome *c* and cytochrome *c* peroxidase determined by paramagnetic NMR. *Proc. Natl. Acad. Sci. U. S. A. 103*, 18945–18950.

(19) Bashir, Q., Volkov, A. N., Ullmann, G. M., and Ubbink, M. (2010) Visualization of the encounter ensemble of the transient electron transfer complex of cytochrome *c* and cytochrome *c* peroxidase. *J. Am. Chem. Soc. 132*, 241–247.

(20) Erman, J. E., Vitello, L. B., Pearl, N. M., Jacobson, T., Francis, M., Alberts, E., Kou, A., and Bujarska, K. (2015) Binding of yeast cytochrome *c* to forty-four charge-reversal mutants of yeast cytochrome *c* peroxidase: isothermal titration calorimetry. *Biochemistry 54*, 4845–4854.

(21) Pearl, N. M., Jacobson, T., Arisa, M., Vitello, L. B., and Erman, J. E. (2007) Effect of single-site charge-reversal mutations on the catalytic properties of yeast cytochrome *c*

peroxidase: Mutations near the high-affinity cytochrome *c* binding site. *Biochemistry 46*, 8263–8272.

(22) Pearl, N. M., Jacobson, T., Meyen, C., Clementz, A. G., Ok, E. Y., Choi, E., Wilson, K., Vitello, L. B., and Erman, J. E. (2008) Effect of single-site charge-reversal mutations on the catalytic properties of yeast cytochrome *c* peroxidase: Evidence for a single, catalytically active, cytochrome *c* binding domain. *Biochemistry 47*, 2766–2775.

(23) Di Savino, A., Foerster, J., La Haye, T., Blok, A., Timmer, M., Ullmann, M., and Ubbink, M. (2020) Efficient encounter complex formation and electron transfer to cytochrome *c* peroxidase with an additional, distant electrostatic binding site. *Angew. Chemie Int. Ed. 132*, 23239–23243.

(24) Di Savino, A., Foerster, J. M., Ullmann, G. M., and Ubbink, M. (2021) The charge distribution on a protein surface determines whether productive or futile encounter complexes are formed. *Biochemistry 17*, 60(10), 747–755.

(25) Volkov, A. N., Bashir, Q., Worrall, J. A. R., Ullmann, G. M., and Ubbink, M. (2010) Shifting the equilibrium between the encounter state and the specific form of a protein complex by interfacial point mutations. *J. Am. Chem. Soc. 132*, 11487–11495.

(26) Volkov, A. N., Bashir, O., Worrall, J. A. R., and Ubbink, M. (2009) Binding hot spot in the weak protein complex of physiological redox partners yeast cytochrome *c* and cytochrome *c* peroxidase. *J. Mol. Biol. 385*, 1003–1013.

(27) Worrall, J. A. R., Kolczak, U., Canters, G. W., and Ubbink, M. (2001) Interaction of yeast iso-1-cytochrome *c* with cytochrome *c* peroxidase investigated by N-15,H-1 heteronuclear NMR spectroscopy. *Biochemistry 40*, 7069–7076.

(28) Worrall, J. A. R., Reinle, W., Bernhardt, R., and Ubbink, M. (2003) Transient protein interactions studied by NMR spectroscopy: The case of cytochrome *c* and adrenodoxin. *Biochemistry 42*, 7068–7076.

(29) Miller, M. A., Liu, R. Q., Hahm, S., Geren, L., Hibdon, S., Kraut, J., Durham, B., and Millett, F. (1994) Interaction domain for the reaction of cytochrome *c* with the radical and the oxyferryl heme in cytochrome *c* peroxidase compound I. *Biochemistry 33*, 8686–8693.

(30) Zhou, J. S., and Hoffman, B. M. (1994) Stern-Volmer in reverse - 2/1 stoichiometry of the cytochrome *c* cytochrome *c* peroxidase electron-transfer complex. *Science (80-.). 265*, 1693–1696.

(31) Van de Water, K., Sterckx, Y. G. J., and Volkov, A. N. (2015) The low-affinity complex of cytochrome *c* and its peroxidase. *Nat. Commun. 6*, 7073.

(32) Matthis, A. L., and Erman, J. E. (1995) Cytochrome *c* peroxidase-catalyzed oxidation of yeast iso-1 ferrocytochrome *c* by hydrogen peroxide. Ionic strength dependence of the steady-state parameters. *Biochemistry 34*, 9985–9990.

(33) Matthis, A. L., Vitello, L. B., and Erman, J. E. (1995) Oxidation of yeast iso-1 ferrocytochrome *c* by yeast cytochrome *c* peroxidase compounds I and II. Dependence

upon ionic strength. *Biochemistry 34*, 9991–9999.

(34) McLendon, G., Zhang, Q., Billstone, V., Wallin, S. A., Miller, R. M., Spears, K. G., and Hoffman, B. M. (1993) Thermodynamic and kinetic aspects of binding and recognition in the cytochrome c/cytochrome c peroxidase complex. *J. Am. Chem. Soc. 115*, 3665–3669.

(35) Van Leeuwen, J. W. (1983) The ionic strength dependence of the rate of a reaction between two large proteins with a dipole moment. *Biochim. Biophys. Acta - Protein Struct. Mol. Enzymol. 743*, 408–421.

(36) Watkins, J. A., Cusanovich, M. A., Meyer, T. E., and Tollin, G. (1994) A "parallel plate" electrostatic model for bimolecular rate constants applied to electron transfer proteins. *Protein Sci. 3*, 2104–2114.

(37) Meyer, T. E., Zhao, Z. G., Cusanovich, M. A., and Tollin, G. (1993) Transient kinetics of electron transfer from a variety of *c*-type cytochromes to plastocyanin. *Biochemistry 32*, 4552–4559.

(38) Suh, J. Y., Tang, C., and Clore, G. M. (2007) Role of electrostatic interactions in transient encounter complexes in protein-protein association investigated by paramagnetic relaxation enhancement. *J. Am. Chem. Soc. 129*, 12954–12955.

(39) Hazzard, J. T., McLendon, G., Cusanovich, M. A., and Tollin, G. (1988) Formation of electrostatically-stabilized complex at low ionic strength inhibits interprotein electron transfer between yeast cytochrome *c* and cytochrome *c* peroxidase. *Biochem. Biophys. Res. Commun. 151*, 429–434.

(40) Bernal-Bayard, P., Molina-Heredia, F. P., Hervás, M., and Navarro, J. A. (2013) Photosystem i reduction in diatoms: As complex as the green lineage systems but less efficient. *Biochemistry 52*, 8687–8695.

Supporting Information

Materials and Methods

Sample Preparation

S. cerevisiae Cc and CcP and their variants Cc R13A and CcP_B, were expressed and purified as previously described.[1–5] The EPR and the PRE experiments were performed as previously reported.[3,4,6] For PRE analysis, two sets of R_2dia values were obtained: one was obtained using CCPN analysis version 2.4.0 and the second one fitting the resonances to a glore line shape using FuDA (kindly previously provided by Dr. D. Fleming Hansen, University College London). The two sets of R_2dia values were averaged to obtain the final R_2dia, and their standard deviation was reported as error. The PREs were corrected for the percentage of paramagnetic signal of the MTSL tagged CcP (15% for both CcP_A and CcP_B, see Results) and for the fraction of Cc bound to CcP. The percentage of Cc R13A bound to CcP was calculated using the previously reported binding constant.[7] The assignment of the ^{15}N Cc R13A HSQC was obtained comparing the spectrum with the assignment of the wt Cc spectrum[8–10] (BMRB 17845). Several residues, mostly around the mutation site, could not be assigned. The chemical shift perturbations (CSP) were measured by overlaying the HSQC spectra of Cc R13A bound to CcP tagged with the diamagnetic tag MTS to the spectrum of free Cc R13A. The average CSP were calculated as previously reported.[11]

Kinetic experiments

The stopped flow experiments, the simulations of the kinetics and the analysis of the data was performed as previously described.[12] The t-test analysis for significance in difference of ka values is given in Tables S5.3 and S5.4.

Text S5.1. Simulation of the rates for the Cc:CcP_A and CcR13A:CcP_A complexes

The model for the association reaction is given by reaction 1. The observable is the absorbance change associated with the oxidation of ferrous Cc within the complex with Cc.[12]

$$\mathrm{Cc(Fe^{2+})} + \mathrm{CpdI} \underset{k_{-1}}{\overset{k_1}{\rightleftarrows}} \text{Encounter complex} \underset{k_{-2}}{\overset{k_2}{\rightleftarrows}} \text{Stereospecific complex} \xrightarrow{k_{et}} \mathrm{Cc(Fe^{3+})}\text{:CpdII} \qquad \text{reaction 1}$$

The rates constants in reaction 1 for CcP_A in complex with wt Cc or Cc R13A were simulated using equation S1:

$$k_a = \frac{k_1 k_2 k_{et}}{k_{-2}k_{-1} + k_{-1}k_{et} + k_2 k_{et}} \qquad \text{equation S1}$$

Equation S1 is derived by assuming pseudosteady conditions for the two intermediate states, the encounter complex and the stereospecific complex.

The macroscopic K_D is given by:

$$K_D = \frac{k_{-1}k_{-2}}{k_1 k_2} \qquad \text{equation S2}$$

The fraction of the encounter f_{enc} complex is given by:

$$f_{enc} = \frac{k_{-2}}{k_2 + k_{-2}} \qquad \text{equation S3}$$

At I = 120 mM, k_a, K_D, and f_{enc} have been determined for wt Cc and Cc R13A in complex with wt CcP (CcP_A).([5,7,12]; this work) These values were defined as targets to simulate by varying k_1, k_{-1}, k_2 and k_{-2}. k_{et} was set to 50,000 s^{-1} ([12]) and assumed to be independent of ionic strength. The K_D defines the ratio of k_2 and k_{-2} but not their absolute values. It was assumed that Cc reorients fast within the encounter complex, on a timescale of the rotational diffusion constant (low ns range), but this choice has little effect on the results.

Table S5.1. CSP classes used in the maps. The resonances of ^{15}N CcR13A in complex with CcP_A and CcP_B are listed in descending order (from left to right) according to the shift intensity in ppm. The residues with CSP <0.02 ppm are omitted as their shift intensity is considered not significant.

CcP_A:CcR13A:

≥ 0.06 ppm	Lys 86	Gln 16	His 33	Lys 4	Gly 77	Lys 72	Leu 9	Met 80
0.04-0.06 ppm	Lys 89	Lys 79	Asp 90	Lys 5	Thr 78	Thr 8		
0.02-0.04 ppm	Ser 2	Asp 93	Cys 17	Val 28	Thr 19	Tyr 48	Val 20	Tyr 74
	Glu 88	Val 57	Gln 42	Lys 73	Gly 6	Glu -3	Lys -1	Leu 94
	Asn 70	Lys 87	Lys 100	Ala 7	Ala 3	Phe 82	Leu 98	Lys 54
	Leu 58	Gly 1	Leu 68	Arg 91	Gly 41			
no data	Thr 12	Arg 13	Cys 14	Pro 25	Pro 30	Asn 31	Met 64	Pro 71
	Pro 76	Ala 81	Gly 83	Gly 84				

CcP_B:CcR13A:

≥ 0.06 ppm	Thr 8	Lys 89	Lys 86	Met 80	Gly 6	Leu 94	Asp 93	Gly 77
	Leu 85	Lys 72	Lys 5	His 33	Lys 11	Lys 79	Ser 2	Thr 19
	Gln 16	Phe 10						
0.04-0.06 ppm	Arg 91	Lys 73	Lys -1	Asn 70	Asp 90	Leu 98	Thr 78	Gly 1
	Asn 92							
0.02-0.04 ppm	Lys 87	Ile 53	Val 20	Thr 69	Cys 17	Leu 68	Tyr 74	Ile 75
	Gly 34	Tyr 48	Val 57	Ala 7	Leu 15	Val 28	Phe -2	Thr 49
	Asp 60	Glu -3	Lys 99	Tyr 67	Gly 41	Ala 3	Thr 96	Leu 58
	Glu 21	Asp 50	Glu 66	Ala 43	Ala 0	Trp 59	Lys 54	Thr 102
	Ile 95	Asn 52						
no data	Leu 9	Thr 12	Arg 13	Cys 14	Pro 25	Pro 30	Asn 31	Met 64
	Pro 71	Pro 76	Ala 81	Phe 82	Gly 83	Gly 84	Glu 88	

Table S5.2 Association rate constants ($M^{-1}s^{-1}$) for CcP_A and CcP_B in complex with Cc and Cc R13A. The rate constants and error are calculated as described in [12].

	CcP_A:Cc		CcP_B:Cc		CcP_A:CcR13A		CcP_B:CcR13A	
I (mM)	**k_a**	**st.dev.**	**k_a**	**st.dev.**	**k_a**	**st.dev.**	**k_a**	**st.dev.**
752	6.2E+06	6.0E+05	6.7E+06	8.3E+04	1.3E+06	3.8E+04	1.1E+06	2.5E+04
622	8.2E+06	3.3E+05	1.4E+07	1.7E+06				
502	2.0E+07	1.2E+06	2.8E+07	2.6E+06				
392	4.4E+07	4.5E+06	6.2E+07	9.4E+06				
292	1.3E+08	1.5E+07	2.2E+08	3.1E+07	2.4E+07	2.9E+06	2.4E+07	2.4E+06
192	7.7E+08	8.6E+07	7.5E+08	1.3E+08				
122	1.7E+09	3.0E+08	2.0E+09	2.4E+08	2.3E+08	1.3E+07	3.2E+08	2.5E+07
44	1.7E+09	2.9E+08	1.4E+09	3.2E+08	1.6E+09	1.7E+08	1.7E+09	1.4E+08

Table S5.3. p-values obtained from the t-test performed by comparing the rate of association (*k*(II)) of the Cc:CcP complexes at ionic strength values from 44 mM to 752 mM. The grey boxes indicate p-values > 0.016, meaning that the difference in the rates of association is considered not to be significant. Bonferroni correction was applied using $p < 0.05$ for individual comparisons and $n = 3$ for the number of comparisons for each variant.

I (mM)	CcP_A:Cc/CcP_B:Cc	CcP_A:Cc /CcP_A: CcR13A	CcP_A:Cc/CcP_B: CcR13A
752	3.3E-01	1.0E-07	6.7E-08
292	1.3E-06	6.7E-12	1.4E-11
122	7.6E-02	8.7E-06	1.3E-05
44	4.5E-02	3.8E-01	8.8E-01

I (mM)	CcP_B:Cc/CcP_A: CcR13A	CcP_B:Cc /CcP_B:CcR13A	CcP_A:CcR13A/CcP_B: CcR13A
752	2.5E-08	2.5E-08	2.4E-04
292	2.1E-10	2.4E-10	1.0E+00
122	4.2E-07	5.4E-07	7.2E-06
44	1.0E-01	2.8E-02	5.6E-01

Table S5.4. Number of independent simulations performed to calculate the rate constants *k*(II) and used in t-test.

I (mM)	CcP_A:Cc	CcP_B:Cc	CcP_A:CcR13A	CcP_B:CcR13A
752	12	8	8	8
622	7	8		
502	12	16		
392	8	15		
292	14	14	10	10
192	12	12		
122	8	8	12	8
44	8	8	8	10

Table S5.5. Estimated rate constants for the Cc:CcP_A and CcR13A:CcP_A complexes at 122 mM (11 $mM^{1/2}$) and 44 mM (7 $mM^{1/2}$) ionic strength.

	wtCc:CcPA 11 $mM^{1/2}$	Target	CcR13A:CcPA 11 $mM^{1/2}$	Target	wtCc:CcPA 7 $mM^{1/2}$	Target	CcR13A:CcPA 7 $mM^{1/2}$	Target
k_1 ($M^{-1}s^{-1}$)	2.00E+09		8.00E+08		3.00E+09		1.95E+09	
k_{-1} (s^{-1})	2.30E+04		3.10E+04		2.50E+03		2.50E+03	
k_2 (s^{-1})	6.00E+07		1.70E+07		5.00E+06		1.70E+07	
k_{-2} (s^{-1})	2.60E+07		7.00E+07		7.00E+07		7.00E+07	
k_{et} (s^{-1})	5.00E+04		5.00E+04		5.00E+04		5.00E+04	
K_D (M)	4.98E-06	5.00E-06	1.60E-04	1.66E-04	1.17E-05		5.28E-06	
k_a ($M^{-1}s^{-1}$)	1.67E+09	1.66E+09	2.25E+08	2.26E+08	1.76E+09	1.74E+09	1.62E+09	1.62E+09
fraction encounter	0.30	0.30	0.80	0.80	0.93		0.80	
time E>S, k_2^{-1} (ns)	16.67		58.82		200.00		58.82	
k_a(R13A)/k_a(wt)			0.14	0.14			0.93	0.93

References

(1) Volkov, A. N., Worrall, J. A. R., Holtzmann, E., and Ubbink, M. (2006) Solution structure and dynamics of the complex between cytochrome *c* and cytochrome *c* peroxidase determined by paramagnetic NMR. *Proc. Natl. Acad. Sci. U. S. A. 103*, 18945–18950.

(2) Goodin, D. B., Davidson, M. G., Roe, J. A., Mauk, A. G., and Smith, M. (1991) Amino-acid substitutions at tryptophan-51 of cytochrome *c* peroxidase - Effects on coordination, species preference for cytochrome *c*, and electron-transfer. *Biochemistry 30*, 4953–4962.

(3) Schilder, J., Lohr, F., Schwalbe, H., and Ubbink, M. (2014) The cytochrome *c* peroxidase and cytochrome *c* encounter complex: The other side of the story. *Febs Lett. 588*, 1873–1878.

(4) Di Savino, A., Foerster, J., La Haye, T., Blok, A., Timmer, M., Ullmann, M., and Ubbink, M. (2020) Efficient encounter complex formation and electron transfer to cytochrome *c* peroxidase with an additional, distant electrostatic binding site. *Angew. Chemie Int. Ed. 132*, 23239–23243.

(5) Volkov, A. N., Bashir, O., Worrall, J. A. R., and Ubbink, M. (2009) Binding hot spot in the weak protein complex of physiological redox partners yeast cytochrome *c* and cytochrome *c* peroxidase. *J. Mol. Biol. 385*, 1003–1013.

(6) Bashir, Q., Volkov, A. N., Ullmann, G. M., and Ubbink, M. (2010) Visualization of the encounter ensemble of the transient electron transfer complex of cytochrome *c* and cytochrome *c* peroxidase. *J. Am. Chem. Soc. 132*, 241–247.

(7) Volkov, A. N., Bashir, Q., Worrall, J. A. R., Ullmann, G. M., and Ubbink, M. (2010) Shifting the equilibrium between the encounter state and the specific form of a protein complex by interfacial point mutations. *J. Am. Chem. Soc. 132*, 11487–11495.

(8) Gao, Y., Boyd, J., Williams, R. J. P., and Pielak, G. J. (1990) Assignment of proton resonances, identification of secondary structural elements, and analysis of backbone chemical shifts for the C102T variant of yeast iso-1-cytochrome *c* and horse cytochrome *c*. *Biochemistry 29*, 6994–7003.

(9) Fetrow, J. S., and Baxter, S. M. (1999) Assignment of 15N chemical shifts and 15N relaxation measurements for oxidized and reduced iso-1-cytochrome *c*. *Biochemistry 38*, 4480–4492.

(10) Volkov, A. N., Vanwetswinkel, S., Van de Water, K., and van Nuland, N. A. J. (2012) Redox-dependent conformational changes in eukaryotic cytochromes revealed by paramagnetic NMR spectroscopy. *J. Biomol. Nmr 52*, 245–256.

(11) Grzesiek, S., Bax, A., Clore, G. M., Gronenborn, A. M., Hu, J. S., Kaufman, J., Palmer, I., Stahl, S. J., and Wingfield, P. T. (1996) The solution structure of HIV-1 Nef reveals an unexpected fold and permits delineation of the binding surface for the SH3 domain of Hck tyrosine protein kinase. *Nat. Struct. Biol. 3*, 340–345.

(12) Di Savino, A., Foerster, J. M., Ullmann, G. M., and Ubbink, M. (2021) The charge

distribution on a protein surface determines whether productive or futile encounter complexes are formed. *Biochemistry 17*, 60(10), 747–755.

(13) Geren, L., Hahm, S., Durham, B., and Millett, F. (1991) Photoinduced electron-transfer between cytochrome *c* peroxidase and yeast cytochrome *c* labeled at cys-102 with(4-bromomethyl-4'-methylbipyridine) bis(bypyridine) ruthenium2+. *Biochemistry 30*, 9450–9457.